$x_{ns}$, where $x_{ns}$ is the shock location without particle addition (but with the same nozzle geometry and exit pressure $p_0$ used in the calculation of $\bar{x}_{ns}$), is given by

$$g(\varphi) = \left[\frac{\lambda^2(\lambda-1)}{(\lambda+1)(2\lambda-1)}\,\frac{(\gamma+1)(2\gamma-1)}{\gamma^2(\gamma-1)}\times\frac{\{1+[2/(\lambda-1)\bar{M}_0^2]\}}{\{1+[2/(\gamma-1)M_0^2]\}}\right]^{1/2}\left(\frac{\bar{M}_0}{\bar{M}_9}\right)^2 \quad (13)$$

In some cases, the particles may be sufficiently large so that the flow behind the normal shock may be considered "frozen"; that is, the particles will fail to follow the flow behind the shock. In this event, Eqs. (8, 10, 12, and 13) are replaced by (8f, 10f, 12f, and 13f):

$$\rho/\bar{\rho}_0 = [D(\lambda)/(1+\varphi)]\bar{M}_0^2(R_0/x)^2 \quad (8f)$$

$$\bar{p}_{nsf} = \rho\bar{u}_m^2(2/\gamma+1) \quad (10f)$$

$$\left(\frac{\bar{x}_{ns}}{R_0}\right)_f = \left[\frac{\lambda^2(\lambda-1)\{1+[2/(\lambda-1)\bar{M}_0^2]\}}{(\gamma+1)(2\lambda-1)(1+\varphi)}\,\frac{p_0}{p_\infty}\right]^{1/2}\bar{M}_0^2 \quad (12f)$$

$$g_f(\varphi) = \left[\frac{\lambda^2(\lambda-1)}{(2\lambda-1)(1+\varphi)}\cdot\frac{(2\gamma-1)}{\gamma^2(\gamma-1)}\times\frac{\{1+[2/(\lambda-1)\bar{M}_0^2]\}}{\{1+[2/(\gamma-1)M_0^2]\}}\right]^{1/2}\left(\frac{\bar{M}_0}{\bar{M}_0}\right)^2 \quad (13f)$$

### Results Compared with Experiment

Lewis and Carlson[12] have correlated experimental data showing the change in normal shock location as a function of particle mass-flow ratio $\varphi$. Their data are plotted in Fig. 1 in terms of their $f(\varphi)$, which is just the ratio $\bar{x}_{ns}/x_{ns}$ with no qualification as to particle lag conditions. Since it can be argued that the particle lag in these experiments should be important only behind the normal shock, the present $g_f(\varphi)$ is compared to the experimental data in Fig. 1. (The corresponding values of $g(\varphi)$ are larger than $g_f(\varphi)$ but less than 1.)

Since previous equations are applicable to gas-only flows ($\varphi = 0$; $\lambda = \gamma$), Fig. 2 is included to show the comparison between the present calculation and several other calculations and experiments. The data of Love et al. is found in Ref. 13.

### References


[1] Adamson, T. C., Jr., "The structure of the rocket exhaust plume without reaction at various altitudes," The Univ. of Michigan Institute of Science and Technology Rept. 4613-45-T (June 1963).

[2] Adamson, T. C., Jr. and Nicholls, J. A., "On the structure of jets from highly underexpanded nozzles into still air," J. Aerospace Sci. **26**, 16–24 (1959).

[3] D'Attorre, L. and Harshbarger, F., "Experimental and theoretical studies of underexpanded jets near the mach disc," General Dynamics/Astronautics Rept. GDA-DBE 64-008 (February 19, 1964).

[4] Eastman, D. W. and Radtke, L. P., "Location of the normal shock wave in the exhaust plume of a jet," AIAA J. **1**, 918–919 (1963).

[5] Mirels, H. and Mullen, J. F., "Expansion of gas clouds and hypersonic jets bounded by a vacuum," AIAA J. **1**, 596–602 (1963).

[6] Greifinger, C. and Cole, J., "One-dimensional expansion of a finite mass of gas into a vacuum," Rand Rept. P 2008 (June 6, 1960).

[7] Sedov, L. I., *Similarity and Dimensional Methods in Mechanics* (Academic Press Inc., New York, 1959), pp. 271–281.

[8] Keller, J. B., "Spherical, cylindrical, and one-dimensional gas flows," Quart. Appl. Math. **14**, 171–184 (1956).

[9] Greifinger, C., private communication to R. Foster (February 13, 1963).

[10] Hoglund, R. F., "Recent advances in gas-particle nozzle flows," ARS J. **32**, 662–671 (1962).

[11] Liepmann, H. W. and Roshko, A., *Elements of Gasdynamics* (John Wiley and Sons, Inc., New York, 1957), 1st ed., Chap. II, pp. 51, 53, and 59.

[12] Lewis, C. H., Jr. and Carlson, D. J., "Normal shock location in underexpanded gas and gas-particle jets," AIAA J. **2**, 776–777 (1964).

[13] Love, E. S., Grigsby, C. E., Lee, L. P., and Woodling, M. J., "Experimental and theoretical studies of axisymmetric free jets," NASA TR R-6 (1959).


# Direct Measurement of Velocity by Hot-Wire Anemometry


ANDREW B. BAUER*

*Aeronutronic Applied Research Laboratory, Newport Beach, Calif.*


### Introduction

THIS note reports a new method for measuring fluid velocity. The method is of special interest since it can be combined with the standard hot-wire measurement techniques[1, 2] to determine the fluid pressure $p$, density $\rho$, and temperature $T$, as well as the three velocity components. This is done with a single, small probe.

Standard hot-wire techniques can be used to measure the total temperature $T_0$ and the product $\rho U$, where $U$ is the velocity component normal to the wire, and where the velocity component parallel to the wire is small as compared with $U$. Then additional knowledge of the flow, such as constant density conditions or pitot-static tube measurements, will permit $U$ to be determined. The new method determines $U$ independently, so that $\rho$ is calculated easily. The measurement of $T_0$ then makes it a simple exercise to calculate $T$ and $p$.

The technique makes use of two hot wires mounted on a simple probe. The wires are held parallel to each other. The velocity direction is determined by heating wire no. 1 and sensing the heated wake with wire no. 2, as illustrated in Fig. 1. This is accomplished most easily by first rotating the entire probe through an angle $\varphi$ about an axis parallel to the needle supports. When wire no. 2 is normal to the flow, its temperature and resistance will be a minimum. The resistance is sensed by passing a small constant current through the wire and by measuring the wire voltage. Next, wire no. 1 is moved in the $\bar{y}$ direction until its wake is sensed by a temperature rise in wire no. 2. The position of wire no. 2 with respect to wire no. 1 then determines the flow direction.

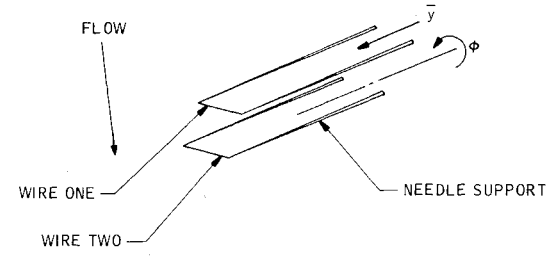


**Fig. 1 Probe schematic diagram; a short current pulse heats wire no. 1, which is moved so that its heated wake is sensed by wire no. 2; the relative positions of the two wires and the time for the heat pulse to reach wire no. 2 determine the velocity vector.**

Received January 4, 1965; revision received March 17, 1965.

* Principal Scientist, Fluid Mechanics Department. Member AIAA.

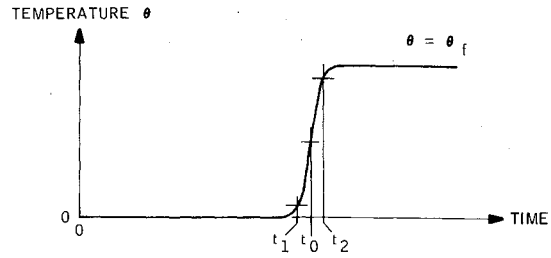


**Fig. 2 Calculated gas temperature at the second wire vs time for a typical probe configuration; at $t_0$ the temperature rise to the final value $\Theta_f$ is 50% completed; at $t_1$ it is 6% completed; at $t_2$ it is 94% completed.**

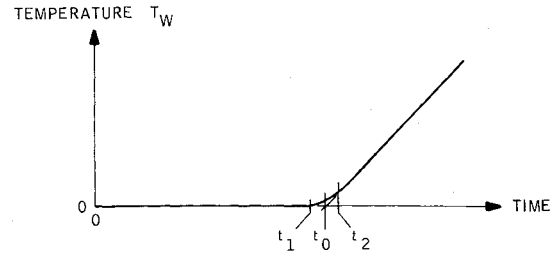


**Fig. 3 Detail of the second-wire temperature-time history illustrating that $t_0$, which is needed to calculate the flow speed, may be found from the straight line after $t_2$ extended to the axis.**

The magnitude of the velocity vector is determined by measuring the time required for a heat pulse to travel from wire no. 1 to wire no. 2. To do this, the steady current used to heat wire no. 1 is replaced by a square-wave current pulse having a length of the order of 1 $\mu$sec. This generates a sharp wake-temperature front, which is convected over the second wire. Because of the wire thermal inertia, the second wire temperature does not jump suddenly from its previous equilibrium value, but it begins an approximately linear rise. This rise is monitored by using an oscilloscope to display the wire voltage, which is a measure of the temperature. Since the distance $h$ between the wires can be made very much larger than the wire diameters, the average velocity in the wire wake is essentially the freestream velocity, and the measured velocity magnitude is

$$U_m = h/t_0 \tag{1}$$

where $t_0$ is the transit time of the heat pulse.

This method has some similarity to the heated-wake velocity measurements of Kovasznay[3] and Sato.[4] Both workers made use of a sine wave to drive the first wire; the second wire had to be moved upstream and downstream to detect the length of one heat wave. Because of the wire thermal inertias, both the first-wire-wake heat amplitude and the second-wire thermal sensitivity would have been reduced greatly except for the fact that Kovasznay and Sato both used low frequencies and small flow speeds. Their air speeds were less than 14 fps.

The present method is expected to be useful at speeds larger by some orders of magnitude, as discussed in this paper. Because both $h$ and $t_0$ are easy to measure, the instrument accuracy is expected to be free of experimental uncertainty or ambiguities; also, the instrument requires no calibration.

## Analysis

For simplicity, the following is limited to considering the first wire as a point heat source in a parallel, uniform, two-dimensional flow. The effect of the heat addition on the flow kinematics is neglected, as it may be shown that the temperature rise in most of the field will be small as compared with ambient for cases of practical interest. If the first-wire temperature jumps by an amount $\Theta_1$ at $t = 0$, it may be shown that the subsequent increase in the freestream temperature $\Theta(x, y, t)$ is given approximately by

$$\Theta(x, y, t) = \frac{Nu\,\Theta_1}{4}\left(\frac{\pi}{R_xPr}\right)^{1/2}\left[\exp\left(-\frac{R_xPry^2}{4x^2}\right)\right]\cdot \left\{\operatorname{erf}\left(\frac{R_xPr}{4}\right)^{1/2} - \operatorname{erf}\left[\left(\frac{R_xPr}{4}\right)^{1/2}\left(1 - \frac{tU}{x}\right)\right]\right\} \tag{2}$$

where $R_x$ = Reynolds number based on $U$ and $x$, $Pr$ = Prandtl number, $Nu$ = Nusselt number, $x$ = coordinate in the freestream direction, $y$ = coordinate normal to $x$, the coordinate origin is at the first wire, and where $R_xPr \gg 1$ and $y/x \ll 1$.

Most of the temperature rise occurs between the times

$$\left.\begin{aligned} t_1 = t_0 - t_e \qquad \text{and} \qquad t_2 = t_0 + t_e \\ \text{where} \qquad t_e = 2t_0/(R_xPr)^{1/2} \end{aligned}\right\} \tag{3}$$

and $t_0$ is now understood to be $x/U$, or the time when the temperature rise is 50% completed. At time $t_1$, the rise is less than 6% completed; at time $t_2$, the rise is more than 94% completed. The temperature after the rise is asymptotic to

$$\Theta_f(x, y) = \frac{Nu\,\Theta_1}{2}\left(\frac{\pi}{R_xPr}\right)^{1/2}\exp\left(-\frac{R_xPry^2}{4x^2}\right) \tag{4}$$

Figure 2 illustrates a typical temperature time history.

An additional rise time is present experimentally because the temperature jump of the first wire is not a square wave. Since the first-wire temperature rise can be made essentially linear, and since the wire time constant or temperature-decay time generally will be long as compared with the temperature rise time at $(x, y)$, Eq. (3) may be replaced by

$$t_1 = t_0 - t_e - t_r \qquad t_2 = t_0 + t_e + t_r \tag{5}$$

where $2t_r$ = the pulse length, and where all of the times are now measured with respect to the center of the initial pulse. These corrected values of $t_1$ and $t_2$ will represent $\Theta(x, y, t)$ to a fair approximation, as sketched in Fig. 2.

The temperature of the sensor wire will not follow $\Theta(x = h, y = 0, t)$ because of the wire thermal inertia. It may be shown that the slope $dT_w/dt$, where $T_w$ is the second-wire temperature, is approximately constant for some period of time after $t_2$; furthermore, the slope before $t_1$ is approximately zero, and $T_w$ follows a smooth curve between $t_1$ and $t_2$. This is illustrated in Fig. 3. The important result is that $t_0$ is given to a good approximation by the intersection of the straight line after $t_2$ with the line of constant temperature before $t_1$. That is, the heat diffusion and the pulse length act to broaden the time between $t_1$ and $t_2$, but they do not affect the intersection at $t_0$.

## Experimental Results

The two-wire method has been tested at Aeronutronic in a small wind tunnel built for this purpose. The wire spacing $h$ was 0.080 in., and the wire diameters were both $10^{-4}$ in. The wire material was 90% Pt and 10% Rh. The pulse amplitude was 50 v; the pulse length, 2 $\mu$sec. The pulse was repeated 50 times/sec; the scope trace photographs are similar to Fig. 3. The measured transit time was 140 $\mu$sec, giving a flow speed of 47 fps. This was checked by a pitot-static tube measurement, which also gave 47 fps.

Work is now in progress to improve the design of the equipment. Then it should be possible to use the probe in flows moving as fast as several thousand feet per second. For example, if $U = 2500$ fps and $h = 10^{-2}$ ft, $t_0 = 4$ $\mu$sec. This would require that the first-wire input pulse have a shorter length (e.g., 0.1 $\mu$sec) so that $t_0$ might be measured with good resolution.

**References**

[1] Liepmann, H. W. and Roshko, A., *Elements of Gasdynamics* (John Wiley and Sons, Inc., New York, 1957), p. 172.

[2] Kovasznay, L. S. G., "Physical measurements in gas dynamics," *High Speed Aerodynamics and Jet Propulsion* (Princeton University Press, Princeton, N. J., 1954), Vol. IX, Sec. F-2.

[3] Kovasznay, L. S. G., "Hot-wire investigation of the wake behind cylinders at low Reynolds numbers," Proc. Roy. Soc. (London) **A198**, 174 (1948).

[4] Sato, H., "Non-linearity and inversion effects of hot-wire anemometer on the mean- and fluctuating-velocity measurements at low wind-speed," Rept. Inst. Sci. Technol. Univ. Tokoyo **11**, 73 (1957).

# Minimum Length MHD Accelerator with Constant Enthalpy

HAROLD MIRELS,* RICHARD R. GOLD,† AND JAMES F. MULLEN‡
*Aerospace Corporation, El Segundo, Calif.*

In a previous note,[1] an analytical solution was presented for the minimum length of a crossed-field magnetohydrodynamic (MHD) accelerator with specified inlet and exit conditions. It was assumed that the flow was one-dimensional, that the working fluid was a perfect gas, that the enthalpy, magnetic field $B$, and electrical conductivity $\sigma$ were each constant, and that the local joule heating was small as compared with the net local electrical power input ($\epsilon R \ll 1$). This solution has been generalized to include variable magnetic field and electrical conductivity. In particular, it has been assumed that

$$\sigma B^2 = \rho^{1-N} \tag{1}$$

where $\rho$ is density and $N$ is a constant. This generalization is outlined here, using the same notation as in Refs. 1 and 2. A brief comparison, with a related analytical solution in Ref. 3, is also made.

Substitution of Eq. (1) into Eq. (7) of Ref. 1 gives

$$x_2 = -\int_1^{u_2} \rho^N \frac{\rho u}{p_1 \rho'}\left[1 + \frac{p_1 \rho'}{\rho u}\right]^2 du \tag{2}$$

which is to be minimized. Equation (2) can be reduced to the same equation that is minimized in Ref. 1 if $\rho^N$ and $p_1/N$ are replaced by $\rho$ and $p_1$, respectively. Hence, Eqs. (8–14) in Ref. 1 are directly applicable to the present problem provided that $\rho$ and $p_1$ therein are replaced by $\rho^N$ and $p_1/N$. If terms of order $\epsilon R$ are neglected,§ then the density variation for a minimum-length accelerator is

$$\rho^N = [1 + \tfrac{2}{3}(N\epsilon/p_1)(u^{3/2} - 1)]^{-1} \tag{3}$$

and the corresponding variation of accelerator length with $u$ is

$$x = (2/3\epsilon)(u^{3/2} - 1) \tag{4}$$

The other dependent variables, to order $\epsilon R \ll 1$, are

$$\left.\begin{aligned} E_y &= uB(1 + \epsilon\rho^N/u^{1/2}) & E_x &= Bj/\sigma\rho = \epsilon(u)^{1/2}/\sigma \\ j &= \rho u^{1/2}\epsilon/B & \omega_e\tau_e &= B/\rho \\ {}_jE_yA &= \epsilon u^{1/2} & \Phi &\equiv -\int_0^x E_x dx = -\int_1^u \frac{u}{\sigma} du \end{aligned}\right\} \tag{5}$$

The area variation is

$$A = 1/\rho u = [1 + (N\epsilon/p_1)\epsilon x]^{1/N}/(1 + \tfrac{3}{2}\epsilon x)^{2/3} \tag{6}$$

For small and large values of $\epsilon x$, respectively,

$$A = 1 + [(\epsilon/p_1) - 1]\epsilon x + O(\epsilon x)^2 \tag{7a}$$

$$= [(N\epsilon/p_1)^{1/N}/(\tfrac{3}{2})^{2/3}](\epsilon x)^{(3-2N)/3N}[1 + O(\epsilon x)^{-1}] \tag{7b}$$

A practical accelerator generally will require $dA/dx \geq 0$. This will require $\epsilon/p_1 \geq 1$ for small $\epsilon x$ and $N \leq \frac{3}{2}$ for large $\epsilon x$.

If the accelerator exit conditions are specified, the required value of $\epsilon/p_1$ is [from Eq. (3)]

$$\epsilon/p_1 = (3/2N)[(\rho_2^{-N} - 1)/(u_2^{3/2} - 1)] \tag{8}$$

The minimum length to achieve these conditions is

$$x_2 = \tfrac{4}{9}(N/p_1)[(u_2^{3/2} - 1)^2/(\rho_2^{-N} - 1)] \tag{9}$$

Equation (9) is of major interest, since it describes the minimum length in terms of the inlet and exit conditions, as well as $N$. The length decreases as $N$ increases.

The variation of conductivity with density for a gas at constant temperature can be approximated generally by $\sigma = \rho^{-N_1}$. For a slightly ionized gas, $\sigma$ is essentially proportional to the degree of ionization. The Saha equation then indicates $0 \leq N_1 \leq \frac{1}{2}$. For a more highly ionized gas, $\sigma$ increases slightly with $\rho$ so that $N_1$ becomes negative. A typical plot of $\sigma$ vs $\rho$ is shown in Fig. 1 for air seeded with potassium. These results were obtained by G. L. Johnston of Aerospace Corporation and permit values of $N_1$ to be obtained for various temperature and density regimes.

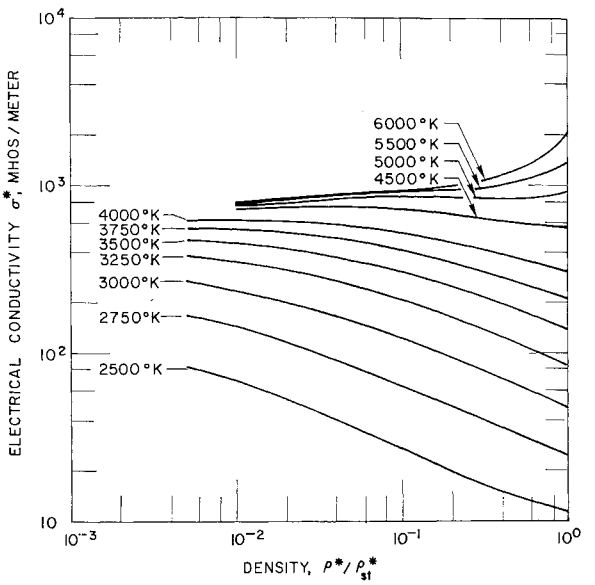


**Fig. 1 Electrical conductivity of air seeded with 0.75% by weight of potassium (symbol $\rho_{st}$* denotes air density at STP).**

Received December 4, 1964; revision received February 18, 1965. This research was supported by the U. S. Air Force under Contract No. AF04(695)-269.

* Head, Advanced Propulsion and Fluid Mechanics Department, Aerodynamics and Propulsion Laboratory. Associate Fellow Member AIAA.

† Head, Magnetogasdynamics Section, Aerophysics Department, Aerodynamics and Propulsion Laboratory; now at Hughes Aircraft Co., Space Systems Division. Associate Fellow Member AIAA.

‡ Member, Technical Staff, Advanced Propulsion and Fluid Mechanics Department, Aerodynamics and Propulsion Laboratory. Member AIAA.

§ A closed-form solution for minimum length can be obtained, without assuming $\epsilon R \ll 1$, for the special case $N = 0$. The resulting solution is

$$\epsilon R = (1 + Cu)^{-1/2}$$

$$\ln\rho = (2/3p_1C^2)[(2 - Cu)(1 + Cu)^{1/2} - (2 - C)(1 + C)^{1/2}]$$

$$x = (2/3C)[(1 + Cu)^{3/2} - 3Cu + 3(1 + Cu)^{1/2}]_{u=1}^{u=u}$$

where $C = (1 - \epsilon^2)/\epsilon^2$.